Single-Molecule Force Spectroscopy of the *Aplysia* Cell Adhesion Molecule Reveals Two Homophilic Bonds

E. Martines,[†△] J. Zhong,[†△] J. Muzard,[†] A. C. Lee,[‡] B. B. Akhremitchev,[§] D. M. Suter,[‡*] and G. U. Lee[†*]

[†]Nanomedicine Centre, School of Chemistry and Chemical Biology, University College Dublin, Dublin, Ireland; [‡]Department of Biological Sciences, Purdue University, West Lafayette, Indiana; and [§]Chemistry Department, Florida Institute of Technology, Melbourne, Florida

ABSTRACT   *Aplysia californica* neurons comprise a powerful model system for quantitative analysis of cellular and biophysical properties that are essential for neuronal development and function. The *Aplysia* cell adhesion molecule (apCAM), a member of the immunoglobulin superfamily of cell adhesion molecules, is present in the growth cone plasma membrane and involved in neurite growth, synapse formation, and synaptic plasticity. apCAM has been considered to be the *Aplysia* homolog of the vertebrate neural cell adhesion molecule (NCAM); however, whether apCAM exhibits similar binding properties and neuronal functions has not been fully established because of the lack of detailed binding data for the extracellular portion of apCAM. In this work, we used the atomic force microscope to perform single-molecule force spectroscopy of the extracellular region of apCAM and show for the first time (to our knowledge) that apCAM, like NCAM, is indeed a homophilic cell adhesion molecule. Furthermore, like NCAM, apCAM exhibits two distinct bonds in the *trans* configuration, although the kinetic and structural parameters of the apCAM bonds are quite different from those of NCAM. In summary, these single-molecule analyses further indicate that apCAM and NCAM are species homologs likely performing similar functions.

INTRODUCTION

Neural cell adhesion molecules regulate a number of key functions during the development of the nervous system, including neuronal migration, axonal growth and guidance, synaptogenesis, and synaptic plasticity as well as axonal regeneration (1–5). These functions depend on the remodeling of the cytoskeleton upon triggering of signal transduction cascades (2). Research into the basic mechanisms of neural cell adhesion molecule regulation and functions may become instrumental for the improvement of devices and treatments aimed at nerve regeneration, cancer therapy, and neuropsychiatric disorders, such as schizophrenia, because neural cell adhesion molecules have been implicated in these disorders (6). An extensive amount of work has been dedicated to study the role of the immunoglobulin superfamily of cell adhesion molecules (IgCAMs), including the vertebrate neural cell adhesion molecule (NCAM), in neural development and regeneration; however, the molecular details of how these molecules trigger cytoskeletal remodeling remain largely unknown. The lack of simple in vitro assays that can recapitulate NCAM-specific signaling cascades in vertebrate neurons has been circumvented by the development of the restrained-bead-interaction assay, which induces adhesion-evoked growth of large *Aplysia* neuronal growth cones (7). Being 10-times larger than their vertebrate counterparts, *Aplysia* growth cones greatly facilitate the visualization of intracellular protein dynamics and cytoskeletal remodeling.

The *Aplysia* cell adhesion molecule (apCAM), the *Aplysia* homolog of NCAM, is present on the surface of *Aplysia* neurons (8) and highly concentrated at growth cone-growth cone contact sites (9). apCAM has been implicated in growth cone steering (7), neurite fasciculation (8,10,11), synapse formation (12,13), and long-term synaptic facilitation (14,15). Clustering of apCAM adhesion receptors induces association of apCAM with the underlying actin cytoskeleton resulting in either coupling to retrograde actin flow or triggering de novo F-actin assembly, depending on the numbers of receptors engaged per unit area (9). Furthermore, when microbeads coated either with apCAM protein or anti-apCAM antibody are positioned onto the peripheral domain of *Aplysia* growth cones and prevented from actin flow coupling by physical restraint using a micropipette, events similar to growth-cone interactions with physiological targets are observed: reduction of retrograde flow rate together with force buildup, central domain, microtubule, and leading-edge advance along the growth cone-bead interaction axis (7). These findings provided the first direct evidence that apCAM mediates directional growth cone movements through a mechanism referred to as "substrate-cytoskeletal coupling" (16,17).

Traditional biochemical approaches provide excellent qualitative and quantitative information on protein-protein interactions; however, they can only measure the average characteristics of large populations of molecules in equilibrium and cannot distinguish between different behaviors of individual proteins (18). Single-molecule force spectroscopy, on the other hand, can investigate the mechanical properties of a single protein as well as the interaction between two molecules, and the atomic force microscope

---

(AFM) has been widely used in this mode to study the strengths of heterophilic (19–24) and homophilic molecular bonds (25–28).

The *Aplysia* cell adhesion molecule apCAM consists of three major isoforms, which differ only in their mode of membrane anchorage: two GPI-linked isoforms with (116 kDa) or without (100 kDa) a glutamate-rich region, and one transmembrane isoform with a cytoplasmic tail (140 kDa). Like NCAM, which shares 30% of its amino-acid sequence with apCAM, the extracellular segment consists of five immunoglobulin-like domains followed by two fibronectin type III (Fn III) repeat domains (10) (Fig. 1, *a* and *b*). However, there is no direct information available on the biochemical or biophysical binding properties of apCAM. While antibody perturbation data support

the hypothesis of homophilic apCAM binding (7,8,10), there is no published record available that provides proof of such binding properties. Using single-molecule AFM force spectroscopy, we present the first direct evidence (to our knowledge) of homophilic apCAM-apCAM *trans*-interactions involving two distinct bonds and characterized their binding properties.

MATERIALS AND METHODS

Materials and reagents

Gold substrates, 200-nm-thick gold film evaporated onto 1-mm glass slides with a 5-nm-thick chromium underlayer, were purchased from Lebow (Goleta, CA). Commercial gold-coated TR400-PB AFM probes were purchased from Olympus (Tokyo, Japan). Polyethylene glycol (PEG, i.e., COOH-PEG-SH, molecular mass: 3.4 kDa) and CH_3O- PEG-SH (mPEG, molecular mass: 2 kDa) were purchased from Creative PEGWorks (Winston Salem, NC). Quantities of 1-step ultra-tetramethylbenzidine substrate, *n*-hydroxysulfosuccinimide, and 1-ethyl-3-(3-dimethylaminopropyl) carbodiimide were purchased from Fisher Scientific Ireland (Dublin, Ireland). Analytical grade chloroform (CHROMASOLV Plus, 99.9%; Sigma-Aldrich, Arklow, Ireland), absolute ethanol, H_2SO_4, H_2O_2, bovine serum albumin (BSA), phosphate-buffered saline (PBS), 2-(*n*-morpholino)ethanesulfonic acid, and TWEEN20 were purchased from Sigma-Aldrich.

Recombinant His6-tagged apCAM containing the extracellular portion was expressed by baculovirus-infected Sf9 cells and purified using nickel-nitrilotriacetic acid agarose, as previously described by Suter et al. (29), with the following modifications. Protein expression and purification was carried out by Kinnakeet Biotechnology (Midlothian, VA). Briefly, Sf9 cells were infected with a baculovirus containing the apCAM construct at multiplicity of infection of 43 for 50 h. After cell harvesting by centrifugation, Sf9 cells were lysed by freezing/thawing and homogenization in hypotonic 20 mM Tris buffer pH 8.5. After salt adjustment of the protein lysate, apCAM was purified over 5 mL of packed nickel-nitrilotriacetic acid agarose column using the following elution buffer: 20 mM Tris-Cl, 100 mM KCl, 100 mM imidazole, 10% glycerol, pH 8.5. The apCAM-containing fractions were dialyzed against PBS/10% glycerol and analyzed for protein concentration by BCA assay and purity by sodium dodecyl sulfate-polyacrylamide gel electrophoresis followed by Coomassie-blue staining and Western blotting with the monoclonal apCAM antibody 4E8, respectively (see Fig. S1 in the Supporting Material). 4E8 IgG was purified as previously described in Suter et al. (7). 4E8 hybridomas were kindly provided by K. Martin, E. Kandel, and S. Schacher (Columbia University, New York, NY).

FIGURE 1 Experimental details of the apCAM-apCAM force spectroscopy measurements. (*a*) Schematic representation of the extracellular Ig1-Ig2-Ig3 domains of apCAM. (*b*) Structural superimposition of the Ig1-Ig2-Ig3 domains of apCAM produced by homology modeling (the domains are represented in *green*, *orange*, and *red color*, respectively) with the crystal structure of the Ig1-Ig2-Ig3 domains of rat NCAM (*blue color*) (38). The following protein accession numbers were used: NCAM (Uniprot No. P13591) and apCAM (Uniprot No. Q9BKP9). (*c*) Schematic of the experimental setup for apCAM-specific force spectroscopy where $m = 77$ and $n = 45$. Approximate PEG (calculated) and apCAM (48) lengths are shown. Schemes are not to scale.

Probe and substrate functionalization

Gold-coated AFM probes and gold substrates were cleaned twice in chloroform for 10 min, then exposed to ozone for 10 min in a UVO/ozone cleaner (Jelight, Irvine, CA), and finally washed three times in chloroform for 10 min. Immediately after the cleaning processes, the AFM probes and gold substrates were immersed into 1 mM COOH-PEG: mPEG 1:200 (mol/mol) solution in chloroform for 12–18 h at room temperature (RT). The PEG-coated surfaces were washed three times with chloroform, three times with absolute ethanol, and three times with Milli-Q water (Millipore, Billerica, MA), and then activated by immersing in a solution of *n*-hydroxysulfosuccinimide (10 mg/mL) and 1-ethyl-3-(3-dimethylaminopropyl) carbodiimide (40 mg/mL) in 2-(*n*-morpholino)ethanesulfonic acid buffer (pH 6) for 30 min at RT. The activated surfaces were washed three times with PBS buffer (pH 7.4) and incubated with 0.2 mg/mL apCAM solution in PBS (pH 7.4) for 2 h at RT. Finally, the functionalized gold probes and surfaces were washed three times with 0.1% TWEEN20 in PBS and stored in PBS (pH 7.4) at 4°C for up to 72 h.

Solid-phase binding assays

Gold-coated substrates were functionalized by linking apCAM to mixed COOH-PEG: mPEG surfaces ranged from 5% to 100% COOH-PEG ratios, and then were blocked with 2% BSA in PBS overnight. apCAM antibody 4E8 (5 μg/mL in PBS/0.05% TWEEN20/0.2% BSA) or monoclonal anti-His6 antibody (Sigma-Aldrich, Arklow, Ireland; 1:200 in PBS/0.05% TWEEN20/0.2%BSA) were incubated in each well for 2 h at RT, and washed with 0.05% TWEEN20/0.2%BSA in PBS. Binding of 4E8 or anti-His6 to apCAM was detected by peroxidase-conjugated human anti-mouse (AbD Serotec, Kidlington, UK), revealed using the 3,3′,5,5′-tetramethylbenzidine (1-step ultra-tetramethylbenzidine substrate; Thermo Scientific, Dublin, Ireland) substrate and quantified with a microplate reader (Biotek Instruments, Winooski, VT) at 450-nm wavelength according to manufacturer's protocol. Nonspecific apCAM binding to mPEG-coated substrates was subtracted to calculate specific binding.

Single-molecule force spectroscopy

Force spectroscopy experiments between apCAM-functionalized cantilevers and apCAM-functionalized gold substrates were performed using an MFP-3D-Bio atomic force microscope (Asylum Research, Santa Barbara, CA) (30). All measurements were performed in 0.2 μm-filtered PBS at RT. Force maps consisting of 32 $\times$ 32 force curves over a 5 $\times$ 5 μm^2 area were collected with a 5-nm relative trigger. For association rate measurements, the dwell (contact) time was varied between 0 and 2 s, while for dissociation measurements it was fixed at 0.2 s. Instant loading rates for the dissociation rate measurements ranged from ~300 to ~14,000 pN/s, while association rate measurements were done at 14,000 pN/s. The spring constants of the cantilevers were determined by thermal fluctuation in air (31).

Data analysis

Data processing and analysis were performed with a custom-written software for MATLAB (The MathWorks, Natick, MA) as described previously in Ray et al. (32). When more than one rupture event was present in a force curve, only the last event was included in the analysis. In order to extract the specific apCAM-apCAM unbinding events associated to PEG stretching, the rupture transitions were fitted with the freely-jointed chain (FJC) model, where the Kuhn length was fixed at 0.7 nm and the contour length was the only fitting parameter (22). Rupture events with a fit error smaller than the experimental noise were deemed specific to apCAM-apCAM unbinding. Histograms of the FJC-filtered contour lengths of the rupture events showed a uniform distribution, therefore no additional filter was applied.

Estimation of the association rate requires the determination of the characteristic interaction time τ and of the effective concentration c_{eff} of apCAM molecules at the AFM probe tip (33). The probability of binding, P_b, is

$$P_b = A \left[1 - \exp \left(\frac{-(t - t_0)}{\tau} \right) \right], \tag{1}$$

where t_0 is the lag time of binding and A is the maximum observable binding probability. Fitting P_b as a function of dwell times in Eq. 1 yielded τ, which in turn was used to estimate k_{on} as

$$k_{on} = \frac{1}{\left(\tau c_{eff} \right)}, \tag{2}$$

where c_{eff} is the inverse of the effective volume covered by one PEG linker, considered as a half-sphere of radius equal to the PEG length.

For dissociation rate measurements, between 32 and 139 specific rupture events per loading rate were extracted and plotted in force histograms. The bin size in the force histograms was determined as 2 $\times$ root-mean-square noise at different loading rates, and ranged from 11 to 26 pN. The most probable rupture forces were derived from the Gaussian fits of the force histograms and plotted against the logarithm of the corresponding loading rates (dynamic force spectra). The unbinding of the apCAM-apCAM complex was analyzed with the Bell model (34,35), which predicts that a pulling force F distorts the energy landscape of the complex, resulting in a lowering of the activation barrier, and consequently an increase in the dissociation rate as

$$k(F) = k_{off} e^{\frac{F x^{\ddagger}}{k_{\mathrm{B}} T}}, \tag{3}$$

where k_{off} is the dissociation rate in the absence of pulling force (thermal dissociation rate), $x^{\ddagger}$ is the separation distance of the transition state from the bound state along the separation path, and $k_{\mathrm{B}} T$ is the thermal energy. In a model with a single energy barrier along the separation path, the most probable unbinding force depends logarithmically on the loading rate (21) as

$$F = \frac{k_{\mathrm{B}} T}{x^{\ddagger}} \ln \left[\frac{x^{\ddagger} r_F}{k_{off} k_{\mathrm{B}} T} \right], \tag{4}$$

where F is the most probable unbinding force and r_F is the instantaneous loading rate on the complex,

$$r_F = \frac{k_c k_t s}{\left(k_c + k_t \right)}, \tag{5}$$

with k_c being the spring constant of cantilever, k_t the instantaneous spring constant of tether at rupture, and s the probe velocity (36). By a linear fit of the data in the dynamic force spectra, it is possible to determine the parameters $x^{\ddagger}$ and k_{off} in Eq. 4. The errors on the fitted parameters were calculated by propagation of uncertainty based on the standard errors of the slope and intercept of the linear Bell-Evans fit. The presence of single and not multiple parallel bonds was verified by comparing the dynamic force spectrum with the predictions of the uncorrelated multiple bond rupture model (22,33),

$$r_F = k_{off} \frac{k_{\mathrm{B}} T}{x^{\ddagger}} \left[\sum_{n=1}^{N} \frac{1}{n^2} e^{\left(-\frac{F x^{\ddagger}}{n k_{\mathrm{B}} T} \right)} \right]^{-1}, \tag{6}$$

where N is the number of bonds.

Homology modeling

The SWISS-MODEL Workspace, a web-based integrated service dedicated to comparative protein structure homology modeling, was used to build the three-dimensional structural model of apCAM Ig1-Ig2-Ig3 domains (37). The x-ray structure of the rat NCAM Ig1-Ig2-Ig3 domains was used as a template (PDB:1QZ1) (38). Observations and three-dimensional visualization were made using PyMol, a user-sponsored molecular visualization system based on an open-source code (39).

RESULTS AND DISCUSSION

apCAM exhibits homophilic binding

apCAM contains five Ig-like extracellular domains, which likely mediate homophilic binding properties, based on

previous NCAM studies suggesting that the first three Ig domains are important for homophilic NCAM interactions (25,38,40–42) (Fig. 1 *a*). Based on structural homology modeling (Fig. 1 *b*), the first three Ig-like domains of apCAM exhibit a similar spatial arrangement as the first three Ig-like domains of rat NCAM (38). However, the two molecules share, at most, 31% identity, and binding studies have not been reported for purified apCAM so far. Therefore, it has been unclear whether apCAM has similar binding properties as NCAM. In this work, AFM-based single-molecule force spectroscopy was used to measure the kinetic parameters of the apCAM-apCAM interaction. PEG linkers were used to functionalize the gold tips and substrates with the complete extracellular portion of apCAM (Fig.1 *c*), because PEGs provide steric mobility for the immobilized protein and minimize nonspecific adhesion. Solid-phase binding assays with the anti-apCAM antibody 4E8 confirmed that apCAM was present on the gold surface (data not shown).

Representative force curves measured between apCAM-functionalized surfaces are depicted in Fig. 2, showing two overlapping force-distance curves with ruptures of different magnitudes. The individual force curves for the separate events are shown as inset traces in Fig. 2. At low forces, <80 pN, the behavior appears to closely follow the FJC behavior for a polymer chain of fixed Kuhn length of 0.7 nm, which is consistent with the extension of PEG linkers (43). However, at higher forces the stretchings before rupture partially deviate from the FJC model at 0.7-nm Kuhn length, which results in an apparent decrease in the Kuhn length. This non-FJC behavior has previously been observed at high force levels in single-molecule AFM measurements, and has been attributed to the extension of the polymer monomers and transition of PEG from a helical phase to a fully extended linear chain. Thus, the high force behavior in Fig. 2 is consistent with our expectations of

previous PEG single molecule measurements and a single apCAM-apCAM interaction (44).

Histograms of the resulting FJC-fitted contour lengths show a Gaussian distribution of contour lengths throughout all the loading rates (Fig. 3 *a* and see Fig. S2) with peaks falling between 38 and 62 nm, which is consistent with the expected contour length of two 3400 MW PEG linkers assembled in series. The frequency distribution of corresponding specific rupture forces were plotted in histograms at a given loading rate, as exemplified in Fig. 3 *b*, revealing two peaks at 70 ± 15 and 126 ± 18 pN, respectively (full list in Fig. S2). The specificity of the interaction was verified by measuring the interaction of apCAM surfaces with BSA- and mPEG-functionalized tips. While the binding probability P_b of the apCAM-apCAM functionalized surfaces varied between 3% and 14%, P_b dropped to 0.5% in the case of BSA-apCAM interaction and to 0.2% in the case of mPEG-apCAM interactions (see Fig. S3). The low binding probability (<14% at 0.2 s dwell time) implies that >90% of the specific measured bond ruptures resulted from single bonds (45,46). In summary, our binding studies using purified recombinant apCAM are the first, to our knowledge, to directly show that this cell adhesion
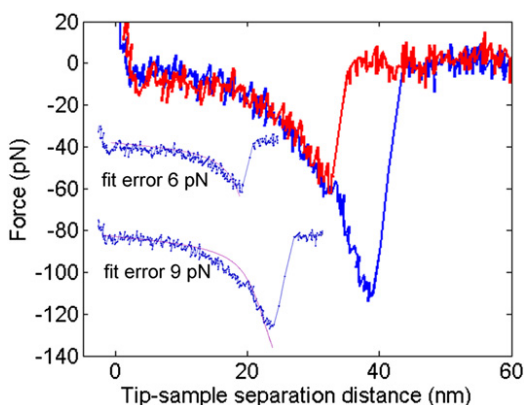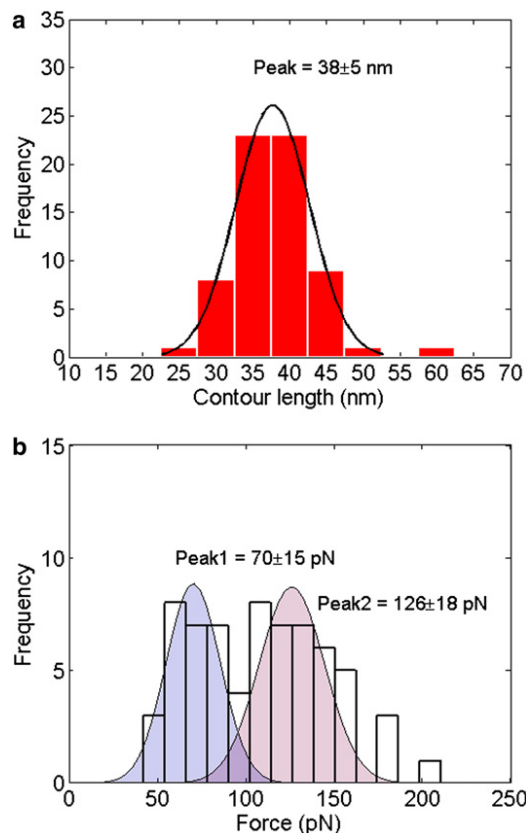

FIGURE 2 Representative force curves at a loading rate of 337 pN/s showing specific ruptures between apCAM that has been covalently immobilized on the surfaces and tips. (*Red and blue color*) Force distribution histograms shown in Fig. 3 *b*. (*Inset*) Same curves with their respective FJC fit to the data (*solid purple lines*) at a fixed Kuhn length of 0.7 nm.

FIGURE 3 (*a*) Representative contour length distribution (obtained at a loading rate of 337 pN/s, *n* = 66) of apCAM-apCAM unbinding events. (*Solid line*) Gaussian fit. (*b*) Specific unbinding force distribution of the rupture events plotted in panel *a*. (*Solid lines*) Gaussian fits (*blue fill*, Peak 1; *red fill*, Peak 2) of the dual distribution shown by the histogram.

molecule indeed undergoes homophilic binding in the *trans* configuration.

apCAM binding through two distinct homophilic bonds

The apCAM-apCAM interaction force histograms were then analyzed as a function of loading rate to determine both bond strengths as well as dissociation and association rate constants. The double Gaussian fit of the force histograms, as exemplified in Fig. 3 *b*, revealed two distinct peaks, suggesting the occurrence of two different types of apCAM-apCAM bonds similar to the case of NCAM (25). These two peaks were identified in all force histograms at all loading rates tested (see Fig. S2), and the rupture force values of both peaks were seen to increase with loading rate. The increase in force with loading rate was very small in the case of the low force peak, which could suggest the observation of equilibrium unbinding (47). However, because the slope of the Bell-Evans model linear fit to this data is not negligible (Fig. 4 *a*), the kinetic parameters of the low force regime extracted with this method, and their propagated errors were calculated (Table 1).

Predictions of the uncorrelated multiple bond-rupture model for a double bond ($N = 2$ in Eq. 6) are also represented in Fig. 4 *a*, showing that the force ruptures from the high force peak do not follow the predicted trend for a double bond when plotted against an uncorrected loading rate. Correction of the loading rate to account for a double bond (22,33) did not provide a better overlap of the data trend (data not shown). Given the low binding probability and despite deviations from the FJC predictions at higher forces, this observation reinforces the claim that the two peaks correspond to two different binding modes of a single-molecule interaction. For this reason, the experimental data from the high-strength regime were also fitted with the Bell-Evans model to extract the corresponding kinetic parameters.

The Bell-Evans fitting of the two sets of peak forces resulted in distinct kinetic parameters. The low-force regime (Peak 1) had a transition distance $x_1^{\ddagger} = 0.46 \pm 0.88$ nm and a dissociation rate $k_{off1} = 0.05 \pm 0.88$ s^{-1}, whereas the high force regime (Peak 2) had a transition distance $x_2^{\ddagger} = 0.1 \pm 0.06$ nm and a dissociation rate $k_{off2} = 0.72 \pm 1$ s^{-1}. The transition distances $x^{\ddagger}$ of the homophilic apCAM bonds measured in this work by single-molecule force spectroscopy are similar to the ones measured for NCAM by Wieland et al. (25) (see Table 1). Given the high uncertainty on k_{off1} due to the low slope of the fit, the numerical value of this off-rate cannot be interpreted. The apCAM-apCAM thermal dissociation rate k_{off2} is one order-of-magnitude lower than for NCAM-NCAM (25). As explained below, the differences in dissociation rate between apCAM and NCAM could be due to sequence differences at the interaction surface.
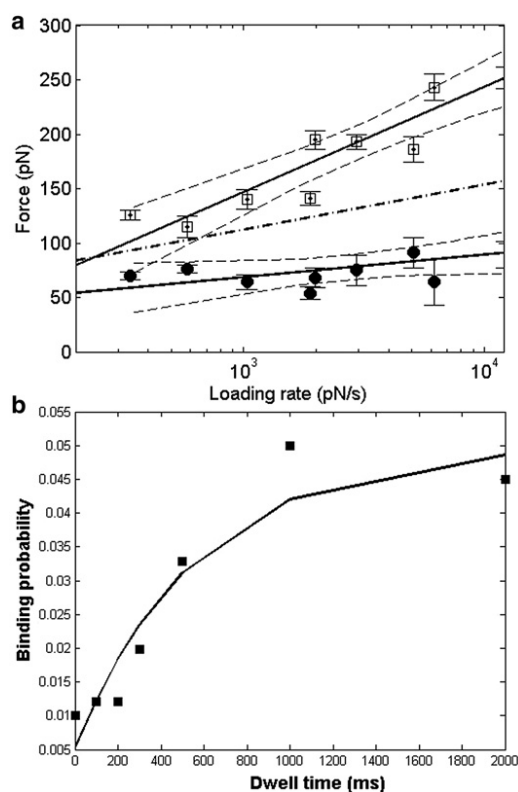

FIGURE 4 (*a*) Dynamic force spectrum of the most probable rupture forces as a function of the corresponding instantaneous loading rates. Data points from Peak 1 (●) and Peak 2 (□) were fitted to the Bell-Evans model (*solid lines*) to extract values of $x^{\ddagger}$ and k_{off}. The error bars represent the width of the Gaussian peak divided by the square-root of the number of unbinding events (21). (*Dashed lines*) 95% confidence bounds. Predictions of the uncorrelated multiple bond rupture model from Eq. 6 are also shown (*dash-dotted line*: Eq. 6 for $N = 2$). (*b*) Binding probability P_b plotted against the dwell time t. The data were fitted to a monoexponential decay as described in the Materials and Methods ($0.05 \times [1-\exp(-(t + 64)/580)]$).

We also determined the association rate for the homophilic apCAM interaction. Fitting of the data to a monoexponential decay (Eq. 1) yielded a contact time $\tau = 580$ ms (Fig. 4 *b*). In turn, assuming a PEG linker stretched at tetrahedral angles and the apCAM length to be 20 nm (48), the effective concentration of molecules c_{eff} at the AFM tip can be estimated to be 5.3×10^4 molecules/μm^3, which results in an association rate $k_{on} \sim 2 \times 10^4$ M^{-1} s^{-1} (upper bound for one single fully stretched PEG molecule). On-rates of similar order of magnitude were measured by

TABLE 1 Comparison of the dynamic parameters of homophilic NCAM bonds (25) and apCAM bonds

	apCAM		NCAM	
	Peak 1	Peak 2	Peak 1	Peak 2
$x^{\ddagger}$ (nm)	0.46 ± 0.88	0.1 ± 0.06	0.3 ± 0.1	0.17 ± 0.04
k_{off} (s^{-1})	0.05 ± 0.88	0.72 ± 1	3.2 ± 0.9	3.2 ± 0.9

Errors of the fit were calculated by propagation of uncertainty based on the standard errors of the slope and intercept of the linear Bell-Evans model fit.

AFM force spectroscopy between *trans*-interacting VE-cadherins (k_{on} ~ 10^3–10^4 M^{-1} s^{-1}).

We calculated the dissociation constant of the high force homophilic apCAM bond to be K_{D2} ~ 4×10^{-5} M. Previous surface plasmon resonance studies have found K_D ~ $5.5 \pm 1.5 \times 10^{-5}$ M (49) between the first two Ig domains of NCAM and K_D ~ 2.5×10^{-8} M between the full-length NCAM ectodomains (50). It would be more meaningful to compare the apCAM-apCAM dissociation constant with the one of NCAM-NCAM obtained by single-molecule force spectroscopy; however, these data are not available at present. However, our calculated values for the dissociation constants of the two homophilic apCAM bonds are also in the range determined for other cell adhesion molecules from other families such as VE-cadherins (26), which are in the range of K_D ~10^{-3}–10^{-6} M. In summary, our results are in agreement with the general observation that homophilic binding of IgCAMs and cadherins represent low-affinity interactions, possibly relying on the formation of multivalent binding blocks as discussed below.

Ig1-Ig3 domains of apCAM and NCAM exhibit a similar structural arrangement

Based on structural, biophysical, biochemical, and cell-cell adhesion data, several binding modes involving mainly the first three Ig domains have been proposed to mediate the homophilic NCAM interactions (25,38,40–42,49–53). Largely because of different NCAM constructs and methods used, these studies have suggested some differences in the way these domains might interact; however, a common picture emerges, suggesting that an intermolecular Ig1-Ig2 interaction as well as another type of binding involving the Ig3 domain are critical for homophilic NCAM interactions. The largest uncertainty, particularly in studies excluding living cells, remains in the question of whether specific domain interactions occur on the same cell surface (*cis*-interaction) or between two opposing cells (*trans*-interaction). Crystal structure data suggest an Ig1-Ig2 *cis*-interaction as well as a *trans*-interaction involving Ig3 with either Ig1 or Ig2, resulting in zipper-like adhesion structures (50). While many studies provide evidence for an Ig1-Ig2 interaction either in *cis* or *trans*, the role of the interaction involving the Ig3 domain is still unclear. However, an Ig2 domain-derived peptide that interferes with the Ig2-Ig3 *trans*-interaction affects neurite outgrowth, neuronal survival, and synaptic plasticity, indicating that the Ig2-Ig3 *trans*-interaction has a biological function (54,55).

Our structural homology modeling revealed that the first three Ig domains of apCAM have a similar secondary structure to NCAM (Fig. 1 *b*). However, when we performed a sequence alignment of the Ig1-3 domains of human NCAM and apCAM we found only 57% similarity and 31% identity in the peptide sequences at the interface between Ig1-Ig2, Ig1-Ig3, and Ig2-Ig3, which can be a reason for the

difference in binding kinetics between NCAM and apCAM homophilic interactions (Fig. 5). The use of deletion mutants in single-molecule force spectroscopy measurements suggested the existence of two distinct NCAM-NCAM binding modes, that were attributed to double-crossed IgG1-IgG2 and IgG3-IgG3 interactions in *trans* (25,50,56). Although our data support the existence of two binding modes for apCAM as well, at present we have no experimental evidence to show which IgG domains might be involved. apCAM, like NCAM, exhibits two homophilic *trans*-bonds of different sensitivity to force, but the parameters that determine the switching from one binding mode to another are still unknown.

Low-affinity interactions are often part of multivalent building blocks, where the strength of adhesion can be rapidly modulated in response to a change of environment (57). Interestingly, several homophilic molecules of the IgCAM family are thought to form zipper-like multivalent systems where they interact both in *cis* and in *trans* (for a review, see Aricescu and Jones (58)). The presence of two homophilic, low affinity apCAM-apCAM binds suggest that this interaction could allow both the fast cell remodeling that underlies growth cone steering and the formation of zipper-like clusters. Formation of such clusters is likely to happen during the initial latency phase of growth-cone interactions with apCAM adhesion substrates; this is when signaling still occurs, but there is little cytoskeletal rearrangement (7,17,29). Future work will determine whether apCAM is capable of forming zipper-like patches like NCAM, while deletion mutants may help elucidate which IgG domains mediate homophilic apCAM-apCAM binding.

CONCLUSIONS

In this work, single-molecule force spectroscopy was used to demonstrate, that apCAM exhibits homophilic binding in *trans* like its presumptive vertebrate homolog, NCAM. Force measurements revealed the existence of two distinct apCAM-apCAM bonds. However, apCAM's relatively low sequence identity to NCAM is paralleled by kinetically different binding properties. apCAM molecules bind with relatively low affinity of K_D~10^{-5} M, which is a common characteristic of homophilic adhesion molecules that form multivalent, zipperlike adhesion patches at the cell surface. Whether apCAM indeed forms zippers at the cell surface is unknown at this point, and it is unclear if zippers can be formed with apCAM molecules that are covalently immobilized on surfaces. This is clearly a subject of future work with live cells. In conclusion, the work in this article supports the idea that homophilic apCAM binding parallels vertebrate NCAM-NCAM interactions, further confirming that apCAM studies in *Aplysia* represent a reliable model system for analyzing cellular NCAM functions with high spatial, temporal, and force resolution.
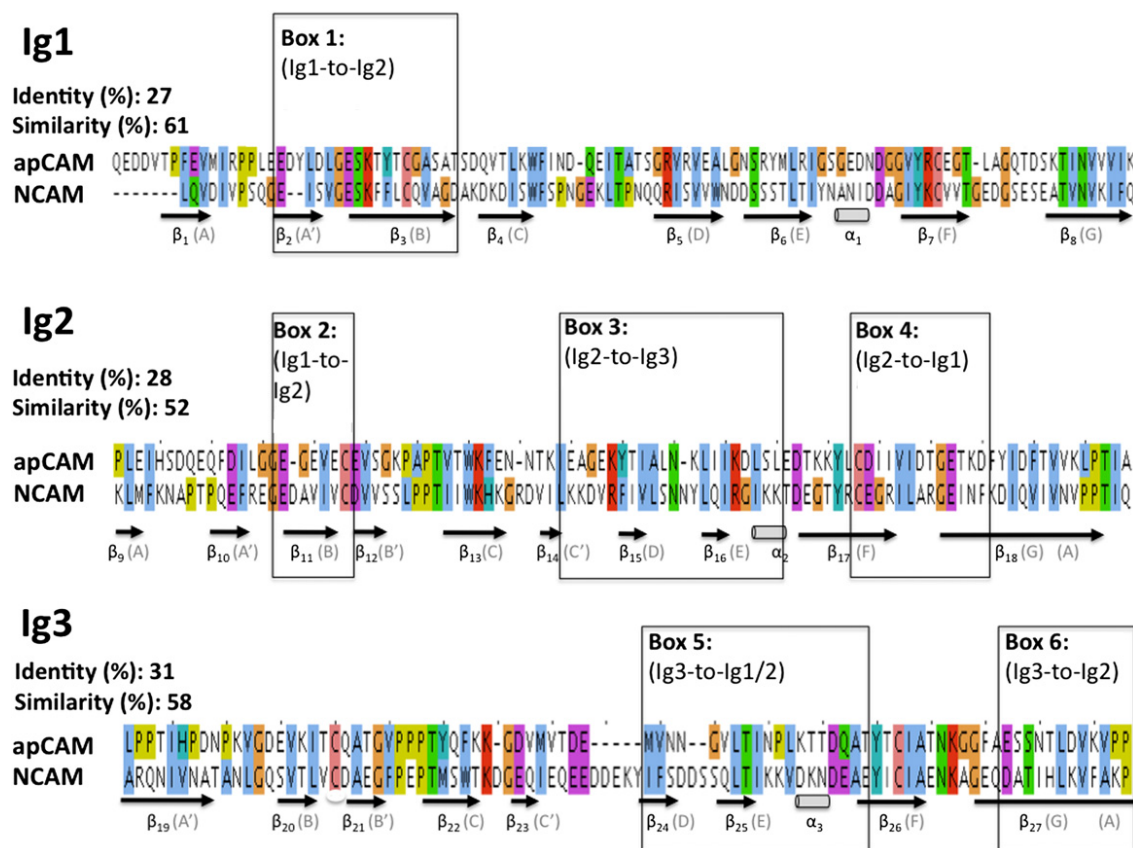
FIGURE 5 Amino-acid sequence alignment of the Ig1, Ig2, and Ig3 domains of human NCAM and *Aplysia* apCAM. Beta-strands are indicated underneath the NCAM sequence. Amino-acid residues are colored according to the Clustal color scheme (*blue*, A, I, L, M, F, W, V, and (C); *red*, R and K; *green*, S, T, N, Q, and (C); *pink*, C; *magenta*, E and D; *orange*, G; *cyan*, H and Y; and *yellow*, P), based on sequence conservation and similarity. Boxes 1–6 highlight NCAM peptide sequences that mediate Ig1-Ig2 as well as Ig3-Ig1 and Ig3-Ig2 domain interactions based on x-ray crystallography and binding data (34,47,49), and exhibit up to 57% similarity and 31% identity (Ig1-Ig2 in box 1) between NCAM and apCAM. This might suggest a possibly conserved binding mechanism between the two cell adhesion molecules. The following protein accession numbers were used: NCAM (Uniprot No. P13591) and apCAM (Uniprot No. Q9BKP9).

SUPPORTING MATERIAL

Three figures are available at http://www.biophysj.org/biophysj/supplemental/S0006-3495(12)00774-6.

REFERENCES

1. Arikkath, J., and L. F. Reichardt. 2008. Cadherins and catenins at synapses: roles in synaptogenesis and synaptic plasticity. *Trends Neurosci.* 31:487–494.

2. Maness, P. F., and M. Schachner. 2007. Neural recognition molecules of the immunoglobulin superfamily: signaling transducers of axon guidance and neuronal migration. *Nat. Neurosci.* 10:19–26.

3. Shapiro, L., J. Love, and D. R. Colman. 2007. Adhesion molecules in the nervous system: structural insights into function and diversity. *Annu. Rev. Neurosci.* 30:451–474.

4. Zipursky, S. L., and J. R. Sanes. 2010. Chemoaffinity revisited: dsCAMs, protocadherins, and neural circuit assembly. *Cell.* 143:343–353.

5. Irintchev, A., and M. Schachner. 2011. The injured and regenerating nervous system: immunoglobulin superfamily members as key players. *Neuroscientist.* 1073858411419047.

6. Brennaman, L., and P. F. Maness. 2008. NCAM in neuropsychiatric and neurodegenerative disorders. *Neurochem. Res.* 10.1007/s11064–008–9630-z.

7. Suter, D. M., L. D. Errante, …, P. Forscher. 1998. The Ig superfamily cell adhesion molecule, apCAM, mediates growth cone steering by substrate-cytoskeletal coupling. *J. Cell Biol.* 141:227–240.

8. Keller, F., and S. Schacher. 1990. Neuron-specific membrane glycoproteins promoting neurite fasciculation in *Aplysia californica*. *J. Cell Biol.* 111:2637–2650.

9. Thompson, C., C. H. Lin, and P. Forscher. 1996. An *Aplysia* cell adhesion molecule associated with site-directed actin filament assembly in neuronal growth cones. *J. Cell Sci.* 109:2843–2854.

10. Mayford, M., A. Barzilai, …, E. R. Kandel. 1992. Modulation of an NCAM-related adhesion molecule with long-term synaptic plasticity in *Aplysia*. *Science.* 256:638–644.

11. Peter, N., B. Aronoff, …, S. Schacher. 1994. Decrease in growth cone-neurite fasciculation by sensory or motor cells in vitro accompanies downregulation of *Aplysia* cell adhesion molecules by neurotransmitters. *J. Neurosci.* 14:1413–1421.

12. Zhu, H., F. Wu, and S. Schacher. 1994. *Aplysia* cell adhesion molecules and serotonin regulate sensory cell-motor cell interactions during early stages of synapse formation in vitro. *J. Neurosci.* 14:6886–6900.

13. Zhu, H., F. Wu, and S. Schacher. 1995. Changes in expression and distribution of *Aplysia* cell adhesion molecules can influence synapse formation and elimination in vitro. *J. Neurosci.* 15:4173–4183.

14. Bailey, C. H., M. Chen, …, E. R. Kandel. 1992. Serotonin-mediated endocytosis of apCAM: an early step of learning-related synaptic growth in *Aplysia*. *Science.* 256:645–649.

15. Lee, S. H., C. S. Lim, …, B. K. Kaang. 2007. Nuclear translocation of CAM-associated protein activates transcription for long-term facilitation in *Aplysia*. *Cell.* 129:801–812.

16. Suter, D. M., and P. Forscher. 1998. An emerging link between cytoskeletal dynamics and cell adhesion molecules in growth cone guidance. *Curr. Opin. Neurobiol.* 8:106–116.

17. Suter, D. M., and P. Forscher. 2000. Substrate-cytoskeletal coupling as a mechanism for the regulation of growth cone motility and guidance. *J. Neurobiol.* 44:97–113.

18. Barkai, E., Y. J. Jung, and R. Silbey. 2004. Theory of single-molecule spectroscopy: beyond the ensemble average. *Annu. Rev. Phys. Chem.* 55:457–507.

19. Hinterdorfer, P., and Y. F. Dufrêne. 2006. Detection and localization of single molecular recognition events using atomic force microscopy. *Nat. Methods.* 3:347–355.

20. Lee, G. U., L. A. Chrisey, and R. J. Colton. 1994. Direct measurement of the forces between complementary strands of DNA. *Science.* 266:771–773.

21. Schwesinger, F., R. Ros, …, A. Pluckthun. 2000. Unbinding forces of single antibody-antigen complexes correlate with their thermal dissociation rates. *Proc. Natl. Acad. Sci. USA.* 97:9972–9977.

22. Sulchek, T. A., R. W. Friddle, …, A. Noy. 2005. Dynamic force spectroscopy of parallel individual Mucin1-antibody bonds. *Proc. Natl. Acad. Sci. USA.* 102:16638–16643.

23. Zhang, X., E. Wojcikiewicz, and V. T. Moy. 2002. Force spectroscopy of the leukocyte function-associated antigen-1/intercellular adhesion molecule-1 interaction. *Biophys. J.* 83:2270–2279.

24. Benoit, M., D. Gabriel, …, H. E. Gaub. 2000. Discrete interactions in cell adhesion measured by single-molecule force spectroscopy. *Nat. Cell Biol.* 2:313–317.

25. Wieland, J. A., A. A. Gewirth, and D. E. Leckband. 2005. Single molecule adhesion measurements reveal two homophilic neural cell adhesion molecule bonds with mechanically distinct properties. *J. Biol. Chem.* 280:41037–41046.

26. Baumgartner, W., P. Hinterdorfer, …, D. Drenckhahn. 2000. Cadherin interaction probed by atomic force microscopy. *Proc. Natl. Acad. Sci. USA.* 97:4005–4010.

27. Wojcikiewicz, E. P., R. R. Koenen, …, V. T. Moy. 2009. LFA-1 binding destabilizes the JAM-A homophilic interaction during leukocyte transmigration. *Biophys. J.* 96:285–293.

28. Panorchan, P., M. S. Thompson, …, D. Wirtz. 2006. Single-molecule analysis of cadherin-mediated cell-cell adhesion. *J. Cell Sci.* 119:66–74.

29. Suter, D. M., A. W. Schaefer, and P. Forscher. 2004. Microtubule dynamics are necessary for SRC family kinase-dependent growth cone steering. *Curr. Biol.* 14:1194–1199.

30. Xiong, Y., A. C. Lee, …, G. U. Lee. 2009. Topography and nanomechanics of live neuronal growth cones analyzed by atomic force microscopy. *Biophys. J.* 96:5060–5072.

31. Hutter, J. L., and J. Bechhoefer. 1993. Calibration of atomic-force microscope tips. *Rev. Sci. Instrum.* 64:1868–1873.

32. Ray, C., S. Guo, …, B. B. Akhremitchev. 2010. Kinetic parameters from detection probability in single molecule force spectroscopy. *Langmuir.* 26:11951–11957.

33. Rankl, C., F. Kienberger, …, P. Hinterdorfer. 2008. Multiple receptors involved in human rhinovirus attachment to live cells. *Proc. Natl. Acad. Sci. USA.* 105:17778–17783.

34. Bell, G. I. 1978. Models for the specific adhesion of cells to cells. *Science.* 200:618–627.

35. Evans, E., and K. Ritchie. 1997. Dynamic strength of molecular adhesion bonds. *Biophys. J.* 72:1541–1555.

36. Ray, C., J. R. Brown, and B. B. Akhremitchev. 2007. Correction of systematic errors in single-molecule force spectroscopy with polymeric tethers by atomic force microscopy. *J. Phys. Chem. B.* 111:1963–1974.

37. Arnold, K., L. Bordoli, …, T. Schwede. 2006. The SWISS-MODEL workspace: a web-based environment for protein structure homology modeling. *Bioinformatics.* 22:195–201.

38. Soroka, V., K. Kolkova, …, C. Kasper. 2003. Structure and interactions of NCAM Ig1-2-3 suggest a novel zipper mechanism for homophilic adhesion. *Structure.* 11:1291–1301.

39. DeLano, W. L. 2002. The PyMOL Molecular Graphics System. DeLano Scientific, San Carlos, CA, USA.

40. Jensen, P. H., V. Soroka, …, F. M. Poulsen. 1999. Structure and interactions of NCAM modules 1 and 2, basic elements in neural cell adhesion. *Nat. Struct. Biol.* 6:486–493.

41. Ranheim, T. S., G. M. Edelman, and B. A. Cunningham. 1996. Homophilic adhesion mediated by the neural cell adhesion molecule involves multiple immunoglobulin domains. *Proc. Natl. Acad. Sci. USA.* 93:4071–4075.

42. Atkins, A. R., M. J. Osborne, …, H. J. Dyson. 1999. Association between the first two immunoglobulin-like domains of the neural cell adhesion molecule N-CAM. *FEBS Lett.* 451:162–168.

43. Oesterhelt, F., M. Rief, and H. Gaub. 1999. Single molecule force spectroscopy by AFM indicates helical structure of poly(ethylene-glycol) in water. *New J. Phys.* 1:6.

44. Sulchek, T., R. W. Friddle, and A. Noy. 2006. Strength of multiple parallel biological bonds. *Biophys. J.* 90:4686–4691.

45. Tees, D. F., R. E. Waugh, and D. A. Hammer. 2001. A microcantilever device to assess the effect of force on the lifetime of selectin-carbohydrate bonds. *Biophys. J.* 80:668–682.

46. Merkel, R., P. Nassoy, …, E. Evans. 1999. Energy landscapes of receptor-ligand bonds explored with dynamic force spectroscopy. *Nature.* 397:50–53.

47. Gomez-Casado, A., H. H. Dam, …, J. Huskens. 2011. Probing multivalent interactions in a synthetic host-guest complex by dynamic force spectroscopy. *J. Am. Chem. Soc.* 133:10849–10857.

48. Becker, J. W., H. P. Erickson, …, G. M. Edelman. 1989. Topology of cell adhesion molecules. *Proc. Natl. Acad. Sci. USA.* 86:1088–1092.

49. Kiselyov, V. V., V. Berezin, …, E. Bock. 1997. The first immunoglobulin-like neural cell adhesion molecule (NCAM) domain is involved in double-reciprocal interaction with the second immunoglobulin-like NCAM domain and in heparin binding. *J. Biol. Chem.* 272:10125–10134.

50. Johnson, C. P., I. Fujimoto, …, D. Leckband. 2004. Mechanism of homophilic adhesion by the neural cell adhesion molecule: use of multiple domains and flexibility. *Proc. Natl. Acad. Sci. USA.* 101:6963–6968.

51. Rao, Y., X. F. Wu, …, C. H. Siu. 1992. Identification of a peptide sequence involved in homophilic binding in the neural cell adhesion molecule NCAM. *J. Cell Biol.* 118:937–949.

52. Walmod, P. S., K. Kolkova, …, E. Bock. 2004. Zippers make signals: NCAM-mediated molecular interactions and signal transduction. *Neurochem. Res.* 29:2015–2035.

53. Kasper, C., H. Rasmussen, …, I. K. Larsen. 2000. Structural basis of cell-cell adhesion by NCAM. *Nat. Struct. Biol.* 7:389–393.

54. Køhler, L. B., V. Soroka, …, E. Bock. 2010. A peptide derived from a *trans*-homophilic binding site in neural cell adhesion molecule induces neurite outgrowth and neuronal survival. *J. Neurosci. Res.* 88:2165–2176.

55. Kraev, I., C. Henneberger, …, C. Sandi. 2011. A peptide mimetic targeting *trans*-homophilic NCAM binding sites promotes spatial learning and neural plasticity in the hippocampus. *PLoS ONE.* 6: e23433.

56. Hukkanen, E. J., J. A. Wieland, …, R. D. Braatz. 2005. Multiple-bond kinetics from single-molecule pulling experiments: evidence for multiple NCAM bonds. *Biophys. J.* 89:3434–3445.

57. Mammen, M., S. K. Choi, and G. M. Whitesides. 1998. Polyvalent interactions in biological systems: implications for design and use of multivalent ligands and inhibitors. *Angew. Chem. Int. Ed.* 37:2755–2794.

58. Aricescu, A. R., and E. Y. Jones. 2007. Immunoglobulin superfamily cell adhesion molecules: zippers and signals. *Curr. Opin. Cell Biol.* 19:543–550.